LETTER

doi:10.1038/nature12596

Genetic identification of a neural circuit that suppresses appetite

Matthew E. Carter[1,2]†, Marta E. Soden[3,4], Larry S. Zweifel[3,4] & Richard D. Palmiter[1,2]

Appetite suppression occurs after a meal and in conditions when it is unfavourable to eat, such as during illness or exposure to toxins. A brain region proposed to play a role in appetite suppression is the parabrachial nucleus[1–3], a heterogeneous population of neurons surrounding the superior cerebellar peduncle in the brainstem. The parabrachial nucleus is thought to mediate the suppression of appetite induced by the anorectic hormones amylin and cholecystokinin[2], as well as by lithium chloride and lipopolysaccharide, compounds that mimic the effects of toxic foods and bacterial infections, respectively[4–6]. Hyperactivity of the parabrachial nucleus is also thought to cause starvation after ablation of orexigenic agouti-related peptide neurons in adult mice[1,7]. However, the identities of neurons in the parabrachial nucleus that regulate feeding are unknown, as are the functionally relevant downstream projections. Here we identify calcitonin gene-related peptide-expressing neurons in the outer external lateral subdivision of the parabrachial nucleus that project to the lateral capsular division of the central nucleus of the amygdala as forming a functionally important circuit for suppressing appetite. Using genetically encoded anatomical, optogenetic[8] and pharmacogenetic[9] tools, we demonstrate that activation of these neurons projecting to the central nucleus of the amygdala suppresses appetite. In contrast, inhibition of these neurons increases food intake in circumstances when mice do not normally eat and prevents starvation in adult mice whose agouti-related peptide neurons are ablated. Taken together, our data demonstrate that this neural circuit from the parabrachial nucleus to the central nucleus of the amygdala mediates appetite suppression in conditions when it is unfavourable to eat. This neural circuit may provide targets for therapeutic intervention to overcome or promote appetite.

The parabrachial nucleus (PBN) contains subpopulations of neurons that regulate taste[10,11], sodium intake[12,13], respiration[14], pain[15,16], thermosensation[17,18] and appetite suppression[1–3,7]. To identify a specific genetic marker for PBN neurons that suppress appetite, we analysed expression of Fos, a surrogate marker of neuronal excitation, after genetic ablation of agouti-related peptide (AgRP) neurons or injection of lithium chloride (LiCl). AgRP neurons were ablated in mice expressing the human diphtheria toxin receptor (DTR) specifically in AgRP neurons ($Agrp^{DTR}$ mice)[19]. Both AgRP neuron ablation (two diphtheria toxin injections at 50 μg kg^{-1}, intramuscular) and LiCl injection (84 mg kg^{-1}, intraperitoneal) induced Fos expression in the outer external lateral subdivision of the PBN (PBelo; Supplementary Fig. 1). To identify a potential genetic marker for these neurons, we consulted the Allen Brain Explorer (http://mouse.brain-map.org)[20] and searched for genes enriched in the PBelo. The top candidate was *Calca*, the gene that encodes calcitonin gene-related peptide (CGRP) and calcitonin by alternative splicing[21]. Indeed, Fos expression in the PBN after ablation of AgRP neurons strongly overlapped with immunohistochemical detection of CGRP (Supplementary Fig. 2), similar to previous reports of coincident expression of Fos and CGRP after injection of LiCl or lipopolysaccharide (LPS)[6,22].

To control gene expression in these neurons, we generated a genetic knock-in mouse expressing Cre recombinase at the *Calca* locus (Supplementary Fig. 3). When these mice were crossed with Cre-dependent TdTomato reporter mice, ubiquitous red fluorescence was detected throughout the brain, probably because of transient Cre expression during development. However, injection of a Cre-dependent adeno-associated virus (AAV) carrying a mCherry reporter directly into the PBN region of adult $Calca^{Cre/+}$ mice (Fig. 1a) resulted in specific expression of mCherry in CGRP-positive neurons in the PBelo (Fig. 1b and Supplementary Figs 4 and 5).

To map activity in PBelo CGRP neurons, we compared virally targeted mCherry fluorescence with Fos following an array of environmental conditions that induced appetite suppression (see Supplementary Fig. 6 for specific conditions used). In the lateral PBN, more than 80% of Fos expression co-localized with CGRP neurons after AgRP neuron ablation, intraperitoneal injection of LiCl, injection of LPS (Fig. 1c–h) or injection of the satiety hormones amylin or cholecystokinin (CCK; Supplementary Fig. 7a–d). In contrast, few Fos-positive neurons were observed in animals injected with saline (Fig. 1i, j), fasted for 24 h or after aversive tail pinching (Supplementary Fig. 7e–h). The percentage of CGRP neurons co-expressing Fos significantly correlated with the reduction in food intake relative to baseline conditions (Fig. 1k, l; see figure legends for *P* values and Supplementary Information for detailed statistical analyses). These results indicate that PBelo CGRP neurons are active during conditions in which appetite is suppressed but not in response to general adverse conditions.

To determine whether transient stimulation of PBelo CGRP neurons is sufficient to reduce food intake, we unilaterally injected AAV carrying a Cre-dependent channelrhodopsin-2 transgene (AAV1 DIO ChR2–mCherry)[8] into the PBN of $Calca^{Cre/+}$ mice (Fig. 2a). Photostimulation reliably induced action potentials in mCherry-positive neurons in acute brainstem slices at several frequencies (20–40 Hz; Supplementary Fig. 8a) and *in vivo* photostimulation at 30 Hz was sufficient to induce expression of Fos (Supplementary Fig. 8b, c). Stimulation of CGRP neurons *in vivo* for 5 min at 30 or 40 Hz (10-ms pulses) significantly and reversibly suppressed food intake during both baseline conditions and after a 24-h fast (Fig. 2b, c and Supplementary Fig. 8d), demonstrating that activating these neurons is sufficient to suppress food intake. Suppression of feeding after photostimulation was rapid (within 5–10 s; Supplementary Video 1) and reversible (mice typically resumed feeding in 5–10 min after photostimulation ceased). Stimulation at these frequencies did not impair movement or cause overt signs of distress (Supplementary Video 1).

To determine the effects of longer-term stimulation of PBelo CGRP neurons, we unilaterally transduced these neurons with AAV carrying a Cre-dependent hM_3Dq–mCherry[9,23] transgene (Fig. 2d). Stimulation of hM_3Dq with clozapine-*N*-oxide (CNO, 1 mg kg^{-1}) induced Fos expression (Supplementary Fig. 9) and suppressed food intake both during baseline conditions and after a 24-h fast (Fig. 2e, f). Chronic stimulation (once every 12 h for 4 d) resulted in a pronounced reduction

[1]Howard Hughes Medical Institute, University of Washington, Seattle, Washington 98195, USA. [2]Department of Biochemistry, University of Washington, Seattle, Washington 98195, USA. [3]Department of Pharmacology, University of Washington, Seattle, Washington 98195, USA. [4]Department of Psychiatry, University of Washington, Seattle, Washington 98195, USA. †Present address: Department of Biology, Williams College, Williamstown, Massachusetts 01267, USA.

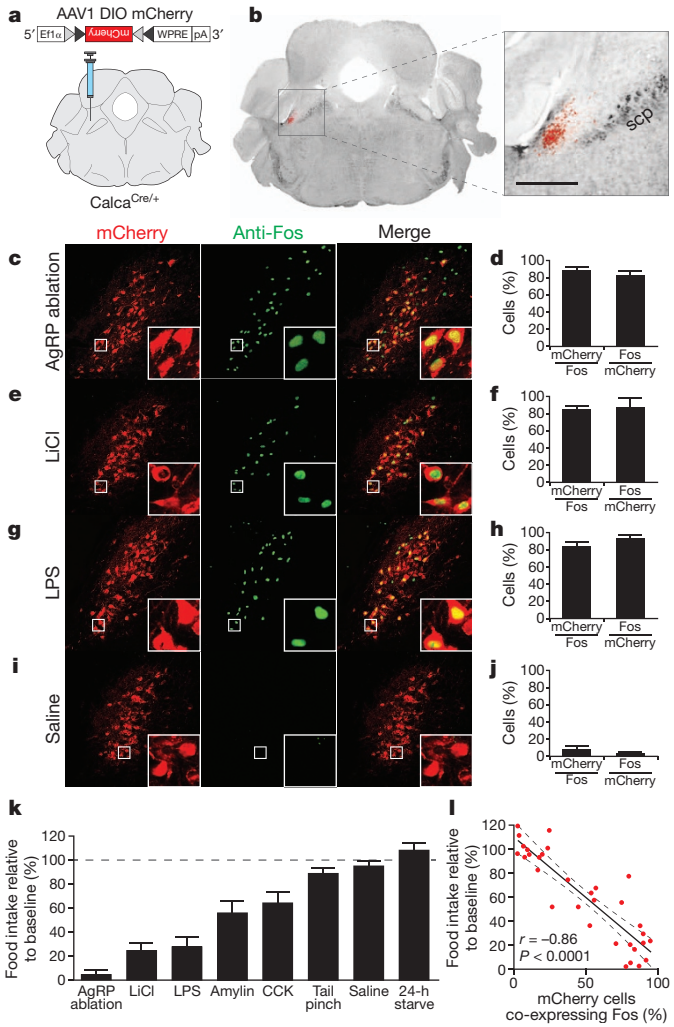

Figure 1 | Co-localization of PBelo CGRP neurons with Fos following conditions that reduce food intake. **a**, AAV carrying a Cre-dependent mCherry reporter injected into the PBN. Grey and black triangles represent loxP and lox2722 sites, respectively. **b**, mCherry expression in the PBelo. scp, superior cerebellar peduncle; scale bar, 500 μm. **c**–**j**, Representative histological examples and quantification of coincidence of mCherry and Fos expression ($n = 4$ animals per condition). **k**, Degree to which various conditions reduce food intake ($n = 4$ animals per condition). **l**, Appetite suppression correlates with the percentage of PBelo CGRP neurons expressing Fos. Dashed lines represent 95% confidence intervals. See Supplementary Information for statistical analysis.

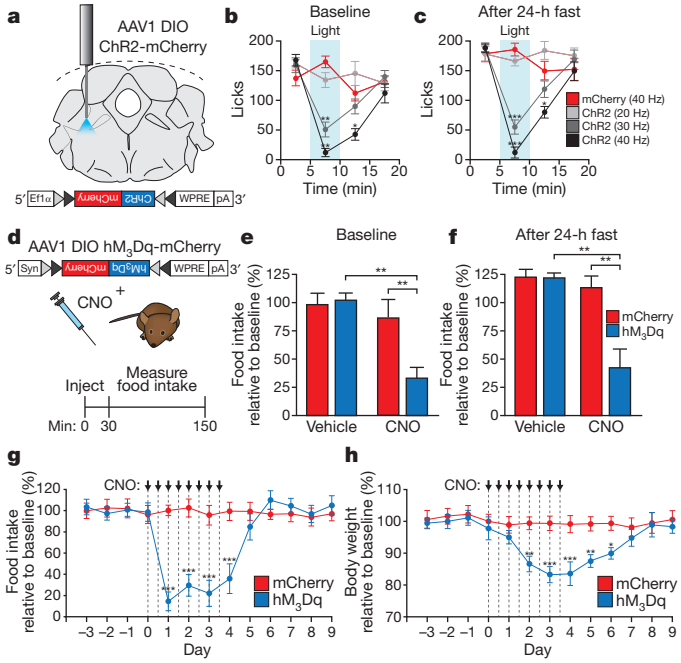

Figure 2 | Stimulation of PBelo CGRP neurons reduces food intake and causes starvation. **a**, Placement of fibre optic implant in the PBN in a $Calca^{Cre/+}$ animal injected with AAV DIO ChR2–mCherry. **b**, **c**, Photostimulation of CGRP neurons reversibly inhibits food intake in both baseline (**b**) and fasted (**c**) conditions ($n = 8$ animals per group); experiment replicated at least 20 times per animal in three groups of animals. **d**, Top, diagram showing AAV DIO hM_3Dq–mCherry transgene unilaterally injected into the PBN; bottom, timeline of experiments in **e**, **f**. **e**, **f**, Pharmacogenetic stimulation of CGRP neurons inhibits food intake in both baseline (**e**) and fasted (**f**) conditions ($n = 6$ animals per group); experiment replicated at least 20 times per animal in three groups of animals. **g**, **h**, Chronic administration of CNO (every 12 h for 4 d) suppresses food intake (**g**) and reduces body weight (**h**) ($n = 6$ animals per group; experiment replicated in three groups of animals). $*P < 0.05$, $**P < 0.01$, $***P < 0.001$; see Supplementary Information for statistical analyses.

in food intake and body weight (Fig. 2g, h), demonstrating that long-term activation of these neurons is sufficient to cause starvation.

To determine the effects of inhibiting PBelo CGRP neurons, we bilaterally transduced these neurons with AAV carrying a Cre-dependent hM_4Di–mCherry[9,23] transgene (Fig. 3a). In acute brainstem slices, bath infusion of CNO reversibly reduced the firing frequency of hM_4Di-expressing neurons to 24.98 ± 8.96% of baseline (Supplementary Fig. 10a, b). There was no change in baseline food intake or body weight after intraperitoneal injection of CNO in either acute or chronic (once every 12 h for 4 d) conditions (Supplementary Fig. 11). However, inhibition of CGRP neurons with CNO decreased the suppression of appetite observed after injection of LiCl or LPS (Fig. 3b). Consistent with this observation, inhibition by hM_4Di also blocked the increase of Fos expression in the PBelo under these conditions (Supplementary Fig. 10c–f). Additionally, inhibition of CGRP neurons with CNO ameliorated appetite suppression after injection of amylin and CCK, although not to statistical significance (Fig. 3b). Because genetic ablation of AgRP neurons induces Fos expression in PBelo CGRP neurons and leads to starvation[7], we considered that bilateral inhibition of CGRP neurons would prevent starvation in these animals. To test this hypothesis, we bred $Agrp^{DTR/+}$ mice with $Calca^{Cre/+}$ mice and bilaterally injected $Agrp^{DTR/+}/Calca^{Cre/+}$ offspring with AAV virus carrying Cre-dependent hM_4Di–mCherry. Indeed, chronic inhibition (injection of CNO every 12 h for 8 d) ameliorated the anorexia and prevented starvation after AgRP neuron ablation (Fig. 3c, d). Taken together, these results demonstrate that inhibition of PBelo CGRP neurons increases food intake under conditions that normally suppress appetite.

To examine the relevant efferent projections of PBelo CGRP neurons, we simultaneously injected two AAV vectors carrying either Cre-dependent mCherry or Cre-dependent synaptophysin–green fluorescent protein (Syn–GFP) transgenes into the PBN of $Calca^{Cre/+}$ mice. We observed dense expression of mCherry- and GFP-positive fibres in the laterocapsular division of the central nucleus of the amygdala (CeAlc; Fig. 4a). This expression overlapped with immunohistochemical detection of CGRP in fibre terminals in the CeAlc (Fig. 4a) and is consistent with previous reports describing projections from the PBN to the central amygdala[16,24,25]. To a lesser degree, we also observed expression of mCherry and Syn–GFP in the bed nucleus of the stria terminalis (BNST; Supplementary Fig. 12). We observed sparse expression of mCherry and Syn–GFP in the lateral hypothalamus, medial thalamus and in the dorsal PBN; expression was notably absent from previously described satiety centres, such as the arcuate nucleus[26] or paraventricular hypothalamus[27]. To confirm the specificity of projections from the PBelo to the CeAlc, we injected green fluorescent retrobeads into the CeAlc and AAV carrying Cre-dependent mCherry in

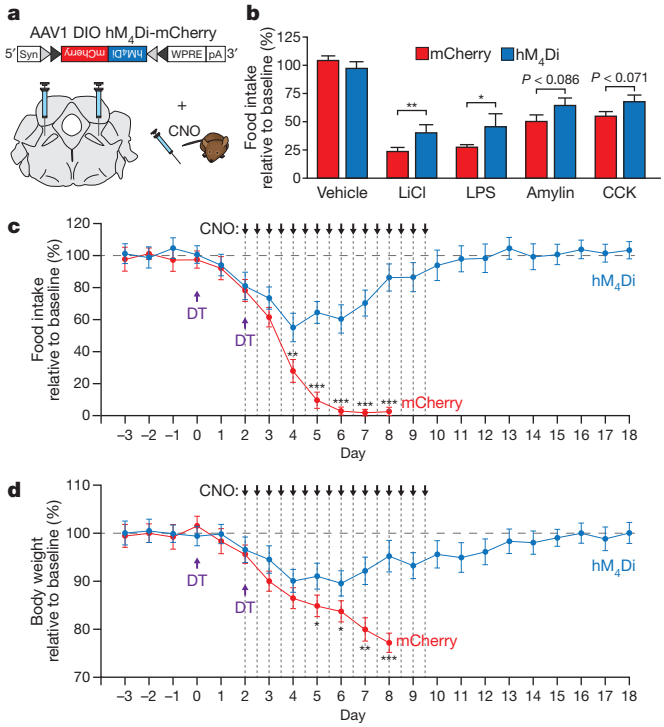

Figure 3 | Inhibition of PBelo CGRP neurons increases food intake during conditions that suppress appetite. **a**, AAV DIO hM_4Di–mCherry transgene bilaterally injected into the PBN. **b**, Pharmacogenetic inhibition of CGRP neurons increases food intake after administration of anorexigenic compounds ($n = 6$ animals per group; experiment replicated at least five times per animal in three groups of animals). **c**, **d**, Chronic administration of CNO (every 12 h for 8 d) increases food intake (**c**) and prevents starvation (**d**) in $Agrp^{DTR/+}$ mice after two injections of diphtheria toxin. The mCherry animals were killed on day 8 owing to extreme weight loss (n =6–9 animals per condition; experiment replicated in three groups of animals). $*P < 0.05$, $**P < 0.01$, $***P < 0.001$; see Supplementary Information for statistical analyses.

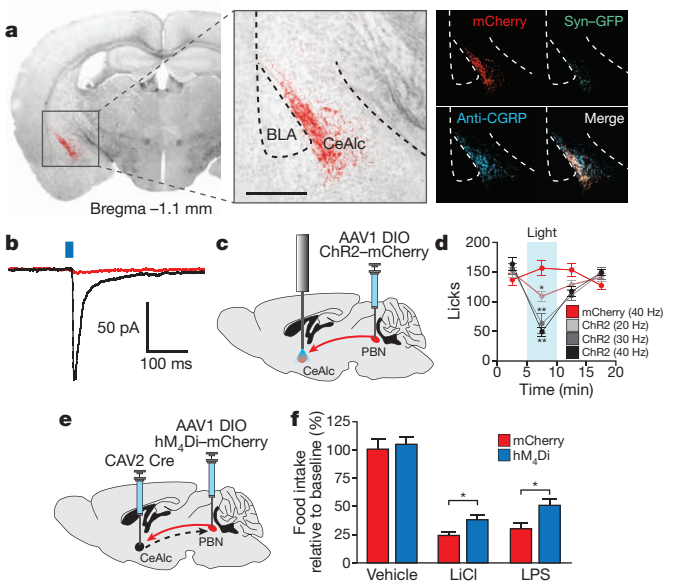

Figure 4 | Efferent projections from PBelo CGRP neurons to the CeAlc mediate appetite suppression. **a**, Left and middle, mCherry-expressing fibres from the PBelo to the CeAlc; scale bar, 500 µm. Right, PBelo fibres expressing mCherry, synaptophysin–GFP and CGRP. **b**, EPSC from a CeAlc neuron upon photostimulation of PBelo-to-CeAlc fibres before (black) and after (red) bath application of CNQX and AP5. **c**, AAV DIO ChR2–mCherry with fibre optic implant above the CeAlc. **d**, Photostimulation of PBelo fibres in the CeAlc reversibly inhibits food intake ($n = 8$ animals for each group; experiment replicated at least 20 times per animal in three groups of animals). **e**, Injection of CAV2 Cre into the CeAlc and AAV DIO hM_4Di–mCherry into the PBN. **f**, Inhibition of retrogradely targeted PBelo neurons increases food intake ($n = 6$ animals for each group); experiment replicated at least five times per animal in three groups of animals. $*P < 0.05$, $**P < 0.01$; see Supplementary Information for statistical analyses.

the PBelo of $Calca^{Cre/+}$ mice. mCherry was expressed in more than 95% of retrogradely labelled green fluorescent neurons (Supplementary Fig. 13).

To demonstrate functional connectivity between the PBelo and the CeAlc, we transduced PBelo CGRP neurons with Cre-dependent ChR2–mCherry. *In vivo* photostimulation of either the PBelo or downstream projections in the CeAlc resulted in an increase in Fos expression in the CeAlc (Supplementary Fig. 14a–f). In acute brain slices, optical stimulation of ChR2–mCherry-positive fibres in the CeAlc resulted in excitatory postsynaptic currents (EPSCs; Fig. 4b and Supplementary Fig. 14g, h) and an increase in firing rate (Supplementary Fig. 14i) in CeAlc neurons (11 out of 25 cells showed an optically evoked response). The EPSCs and the increase in firing rate were blocked by bath application of the glutamate receptor antagonists 6-cyano-7-nitroquinoxaline-2, 3-dione (CNQX; 10 µM) and D(–)-2-amino-5-phosphonovaleric acid (AP5; 50 µM), indicating that PBelo CGRP neurons form an excitatory synaptic connection with neurons of the CeAlc (Fig. 4b and Supplementary Fig. 14g–i). To determine the effect of stimulating PBelo-to-CeAlc projections on food intake, we transduced PBelo CGRP neurons with ChR2–mCherry and implanted fibre optic cannulae above the CeAlc (Fig. 4c). Photostimulation of projections into the CeAlc for 5 min at 20–40 Hz significantly and reversibly suppressed food intake (Fig. 4d and Supplementary Fig. 15). In contrast, stimulation of PBelo projections to the BNST for 5 min had no significant effect on food intake (Supplementary Fig. 16). Taken together, these results indicate that direct projections from PBelo CGRP neurons to the CeAlc are sufficient to reduce food intake.

To determine the necessity of the PBelo-to-CeAlc projection in mediating appetite suppression, we bilaterally injected canine adenovirus (CAV2) carrying Cre recombinase into the CeAlc. CAV2 is capable of efficient retrograde transport[28] and therefore will express Cre in upstream PBelo neurons. In the same animals, we also bilaterally injected AAV carrying a Cre-dependent hM_4Di transgene into the PBN (Fig. 4e). Inhibition of PBN neurons with CNO decreased the suppression of appetite observed after injection of LiCl or LPS (Fig. 4f), demonstrating that activity in PBelo neurons projecting to the CeAlc is necessary for the normal suppression of appetite observed after injection of LiCl or LPS.

Taken together, these results demonstrate a neural circuit from CGRP-expressing neurons in the PBelo to the CeAlc that mediates appetite suppression. One of our observations was that inhibition of PBN neurons increased food intake when mice did not normally eat (Figs 3b–d and 4f), but did not statistically increase food intake in baseline conditions (Supplementary Fig. 11) or after injection of amylin or CCK (Fig. 3b). These findings are consistent with those of Atasoy *et al.*[27], who did not find any effect on food intake after stimulation of inhibitory projections from AgRP neurons to the PBN. Perhaps inhibitory projections from AgRP neurons do not stimulate food intake in baseline conditions but do decrease the suppression of appetite when the PBN is most active. Thus, ablation of AgRP neurons causes starvation in adult mice because of disinhibition in the PBelo[7]. Additionally, PBelo CGRP neurons may not mediate the ordinary, routine satiety experienced after a meal, but may mediate more severe forms of satiety experienced during severe overfeeding (gastric distention), illness or other conditions in which it is unhealthy to eat such as dehydration or vertigo.

Although it is well-established that several hypothalamic and brainstem nuclei coordinate appetite and satiety[26,29], this study demonstrates the involvement of downstream circuitry that may mediate

the 'unpleasant feeling' or discomfort that results from adverse conditions during which it is unfavourable to eat. Indeed, the CeAlc is known to process polymodal information about the internal and external bodily environment including adverse visceral stimuli[30]. Adding to previous results[1,7], we propose that PBelo CGRP neurons integrate visceral and energy balance information and communicate with the CeAlc to mediate extreme satiety and malaise (Supplementary Fig. 17).

METHODS SUMMARY

We generated $Calca^{Cre/+}$ mice and $Agrp^{DTR/+}$ mice and backcrossed them onto a C57Bl/6 background. AAV1 vectors were stereotaxically injected into the PBN; in some experiments, CAV2 Cre was also stereotaxically injected into the CeAlc. For photostimulation experiments, mice were implanted with fibre optic cannulae above the PBN, CeAlc or BNST; blue light at 473 nm was delivered in 10-ms pulses at 20 mW intensity through a 1.5-m fibre optic cable. For pharmacogenetic manipulation, CNO was injected at 1 mg kg^{-1}, intraperitoneally. To ablate AgRP neurons, mice carrying the $Agrp^{DTR/+}$ allele were injected twice with diphtheria toxin (50 μg kg^{-1}, intramuscularly, 2 days apart). LiCl (84 mg kg^{-1}; 0.2 M, 10 ml kg^{-1}), LPS from *Salmonella typhimurium* (50 μg kg^{-1}), amylin (10 μg kg^{-1}) and CCK (10 μg kg^{-1}) were all injected intraperitoneally as described in Supplementary Fig. 6. Food intake was monitored using lickometer cages supplied with water and liquid diet available *ad libitum*.

Online Content Any additional Methods, Extended Data display items and Source Data are available in the online version of the paper; references unique to these sections appear only in the online paper.

Received 1 May; accepted 20 August 2013.
Published online 13 October 2013.

1. Wu, Q., Clark, M. S. & Palmiter, R. D. Deciphering a neuronal circuit that mediates appetite. *Nature* **483,** 594–597 (2012).
2. Becskei, C., Grabler, V., Edwards, G. L., Riediger, T. & Lutz, T. A. Lesion of the lateral parabrachial nucleus attenuates the anorectic effect of peripheral amylin and CCK. *Brain Res.* **1162,** 76–84 (2007).
3. DiPatrizio, N. V. & Simansky, K. J. Activating parabrachial cannabinoid CB1 receptors selectively stimulates feeding of palatable foods in rats. *J. Neurosci.* **28,** 9702–9709 (2008).
4. Yamamoto, T. *et al.* C-fos expression in the rat brain after intraperitoneal injection of lithium chloride. *Neuroreport* **3,** 1049–1052 (1992).
5. Elmquist, J. K., Scammell, T. E., Jacobson, C. D. & Saper, C. B. Distribution of Fos-like immunoreactivity in the rat brain following intravenous lipopolysaccharide administration. *J. Comp. Neurol.* **371,** 85–103 (1996).
6. Paues, J., Mackerlova, L. & Blomqvist, A. Expression of melanocortin-4 receptor by rat parabrachial neurons responsive to immune and aversive stimuli. *Neuroscience* **141,** 287–297 (2006).
7. Wu, Q., Boyle, M. P. & Palmiter, R. D. Loss of GABAergic signaling by AgRP neurons to the parabrachial nucleus leads to starvation. *Cell* **137,** 1225–1234 (2009).
8. Yizhar, O., Fenno, L. E., Davidson, T. J., Mogri, M. & Deisseroth, K. Optogenetics in neural systems. *Neuron* **71,** 9–34 (2011).
9. Armbruster, B. N., Li, X., Pausch, M. H., Herlitze, S. & Roth, B. L. Evolving the lock to fit the key to create a family of G protein-coupled receptors potently activated by an inert ligand. *Proc. Natl Acad. Sci. USA* **104,** 5163–5168 (2007).
10. Rosen, A. M., Victor, J. D. & Di Lorenzo, P. M. Temporal coding of taste in the parabrachial nucleus of the pons of the rat. *J. Neurophysiol.* **105,** 1889–1896 (2011).
11. Tokita, K. & Boughter, J. D. Jr. Sweet-bitter and umami-bitter taste interactions in single parabrachial neurons in C57BL/6J mice. *J. Neurophysiol.* **108,** 2179–2190 (2012).
12. Geerling, J. C. & Loewy, A. D. Sodium deprivation and salt intake activate separate neuronal subpopulations in the nucleus of the solitary tract and the parabrachial complex. *J. Comp. Neurol.* **504,** 379–403 (2007).
13. Geerling, J. C. *et al.* FoxP2 expression defines dorsolateral pontine neurons activated by sodium deprivation. *Brain Res.* **1375,** 19–27 (2011).
14. Chamberlin, N. L. & Saper, C. B. Topographic organization of respiratory responses to glutamate microstimulation of the parabrachial nucleus in the rat. *J. Neurosci.* **14,** 6500–6510 (1994).
15. Hermanson, O. & Blomqvist, A. Subnuclear localization of FOS-like immunoreactivity in the rat parabrachial nucleus after nociceptive stimulation. *J. Comp. Neurol.* **368,** 45–56 (1996).
16. Richard, S., Engblom, D., Paues, J., Mackerlova, L. & Blomqvist, A. Activation of the parabrachio-amygdaloid pathway by immune challenge or spinal nociceptive input: a quantitative study in the rat using Fos immunohistochemistry and retrograde tract tracing. *J. Comp. Neurol.* **481,** 210–219 (2005).
17. Nakamura, K. & Morrison, S. F. A thermosensory pathway that controls body temperature. *Nature Neurosci.* **11,** 62–71 (2008).
18. Nakamura, K. & Morrison, S. F. A thermosensory pathway mediating heat-defense responses. *Proc. Natl Acad. Sci. USA* **107,** 8848–8853 (2010).
19. Luquet, S., Perez, F. A., Hnasko, T. S. & Palmiter, R. D. NPY/AgRP neurons are essential for feeding in adult mice but can be ablated in neonates. *Science* **310,** 683–685 (2005).
20. Ng, L. *et al.* An anatomic gene expression atlas of the adult mouse brain. *Nature Neurosci.* **12,** 356–362 (2009).
21. Jacobs, J. W. *et al.* Calcitonin messenger RNA encodes multiple polypeptides in a single precursor. *Science* **213,** 457–459 (1981).
22. Paues, J., Engblom, D., Mackerlova, L., Ericsson-Dahlstrand, A. & Blomqvist, A. Feeding-related immune responsive brain stem neurons: association with CGRP. *Neuroreport* **12,** 2399–2403 (2001).
23. Krashes, M. J. *et al.* Rapid, reversible activation of AgRP neurons drives feeding behavior in mice. *J. Clin. Invest.* **121,** 1424–1428 (2011).
24. D'Hanis, W., Linke, R. & Yilmazer-Hanke, D. M. Topography of thalamic and parabrachial calcitonin gene-related peptide (CGRP) immunoreactive neurons projecting to subnuclei of the amygdala and extended amygdala. *J. Comp. Neurol.* **505,** 268–291 (2007).
25. Schwaber, J. S., Sternini, C., Brecha, N. C., Rogers, W. T. & Card, J. P. Neurons containing calcitonin gene-related peptide in the parabrachial nucleus project to the central nucleus of the amygdala. *J. Comp. Neurol.* **270,** 416–426 (1988).
26. Elmquist, J. K., Coppari, R., Balthasar, N., Ichinose, M. & Lowell, B. B. Identifying hypothalamic pathways controlling food intake, body weight, and glucose homeostasis. *J. Comp. Neurol.* **493,** 63–71 (2005).
27. Atasoy, D., Betley, J. N., Su, H. H. & Sternson, S. M. Deconstruction of a neural circuit for hunger. *Nature* **488,** 172–177 (2012).
28. Soudais, C., Laplace-Builhe, C., Kissa, K. & Kremer, E. J. Preferential transduction of neurons by canine adenovirus vectors and their efficient retrograde transport *in vivo*. *FASEB J.* **15,** 2283–2285 (2001).
29. Gao, Q. & Horvath, T. L. Neurobiology of feeding and energy expenditure. *Annu. Rev. Neurosci.* **30,** 367–398 (2007).
30. Neugebauer, V., Li, W., Bird, G. C. & Han, J. S. The amygdala and persistent pain. *Neuroscientist* **10,** 221–234 (2004).

Supplementary Information is available in the online version of the paper.

Acknowledgements We thank B. Roth for hM_3Dq–mCherry and hM_4Di–mCherry constructs, and K. Deisseroth for mCherry and ChR2–mCherry constructs. E. Allen, J. Resnick, M. Soleiman and S. Padilla assisted with histology, E. Allen and A. Rainwater assisted with animal husbandry, and J. Shulkin provided suggestions and advice. We thank members of the Palmiter and Zweifel laboratories for feedback on the manuscript. M.E.C. is financed by a fellowship from the Hilda and Preston Davis Foundation. L.S.Z. is financed by a grant from the National Institutes of Health (R01MH094536). R.D.P is supported in part by grants from the National Institutes of Health (R01DA024908) and the Klarman Family Foundation.

Author Contributions M.E.C. and R.D.P. conceived and designed the study. M.E.C. performed and analysed histological and behavioural experiments, M.E.S. performed electrophysiology experiments and R.D.P. generated $Calca^{Cre}$ knock-in mice. L.S.Z. and R.D.P. provided equipment, reagents and expertise. M.E.C. wrote the manuscript in collaboration with the other authors.

Author Information Reprints and permissions information is available at www.nature.com/reprints. The authors declare no competing financial interests. Readers are welcome to comment on the online version of the paper. Correspondence and requests for materials should be addressed to R.D.P. (palmiter@uw.edu).

METHODS

Mice. All experiments were approved by the University of Washington Institutional Animal Care and Use Committee and were performed in accordance with the guidelines described in the US National Institutes of Health Guide for the Care and Use of Laboratory Animals. We used exclusively heterozygous male *Calca*$^{Cre/+}$ and *Agrp*$^{DTR/+}$ mice backcrossed onto a C57Bl/6 background, aged 7–9 weeks at the start of experimental procedures and no more than 18 weeks at the end of experimental procedures. Before stereotaxic surgery, mice were group housed and maintained with rodent diet (Picolab, number 5053) and water available *ad libitum* with a 12-h light:dark cycle at 22 °C. After surgical procedures, mice were individually housed and maintained with a liquid diet (Vanilla Ensure, Abbot Laboratories) and water available *ad libitum*. We performed experiments on three or four experimental animals (for example, animals transduced with ChR2, hM_3Dq, hM_4Di) and three or four control animals (for example, animals only transduced with mCherry) at the same time to avoid differences in results between experimental sessions. Animals were randomly assigned to either the experimental or control groups in each litter.

Generation of *Calca*^{Cre} mice. A 14-kb BstB1–Pac1 fragment was isolated from a C57Bl/6 mouse BAC clone. A unique Sal1 site was introduced at the initiation codon of *Calca* in exon 2 by PCR. Next, a 7-kb Spe1–Sal1 5′ fragment was cloned into a targeting vector containing a *frt*-flanked *PkgNeo* gene for positive selection and Pgk-DTA and HSV-TK genes for negative selection. This was followed by insertion of a 3′ 7-kb Sal1–Pac1 fragment. The gene encoding the Cre–GFP fusion protein with an amino (N)-terminal myc-tag and nuclear localization signal was cloned into the unique Xho1 site adjacent to *frt-PgkNeo*. The targeting construct was linearized with Asc1 and electroporated into G4 hybrid (C57Bl/6 × Sv129) embryonic stem cells. Eighteen correctly targeted clones were identified out of 96 by Southern blot of EcoRV-digested DNA using a unique probe outside the targeting vector. Several of these clones gave good chimaeras when injected into C57Bl/6 hosts. One chimaera was bred with FLPer (Rosa26-Flip recombinase) to remove the *frt–Pgk–Neo* gene.

Virus production. Cre-dependent pAAV mCherry and ChR2–mCherry (driven by the Ef1α promoter) DNA plasmids were provided by K. Deisseroth, and Cre-dependent pAAV hM_3Dq–mCherry and hM_4Di–mCherry (driven by the human synapsin promoter) DNA plasmids were provided by B. Roth. pAAV synaptophysin–GFP was generated by fusing the 3′ end of the mouse *Synaptophysin* coding region with the 5′ end of the *GFP* coding region. This sequence was then exchanged with mCherry in the pAAV mCherry plasmid to make the transgene Cre-dependent. Recombination-deficient AAV vectors were prepared in human embryonic kidney (HEK293T) cells with AAV1 coat serotype, purified by sucrose and CsCl gradient centrifugation steps, and re-suspended in 1× Hanks Balanced Saline Solution (HBSS) at a titre of approximately 2×10^9 viral genomes per microlitre. CAV2 Cre was prepared in dog kidney (DK/E1-1) cells, purified by sucrose and CsCl gradient centrifugation steps, and re-suspended in 1× HBSS at a titre of approximately 2.5×10^9 viral genomes per microlitre as described previously[31]. Viral aliquots were stored at −80 °C before stereotaxic injection.

Stereotaxic surgery. At the start of surgical procedures, mice were anaesthetized with isofluorane and placed on a stereotaxic frame (David Kopf Instruments). Stereotaxic coordinates for the anterior–posterior plane were normalized using a correction factor (F = (Bregma − Lamda distance)/4.21) on the basis of the coordinates of Paxinos and Franklin[32]. Virus was injected unilaterally (on the left side) or bilaterally as described in the text either in the PBN (antero-posterior (AP), −4.9 mm; medio-lateral (ML), 1.4 mm; dorso-ventral (DV), 3.8 mm) or the CeAlc (AP, −1.2 mm; ML, 2.6 mm; DV, 5.4 mm) at a rate of 0.2 μl min^{-1} for 2.5 min (0.5 μl total volume). Note that the viral injection coordinates target the most anterior aspect of the PBN but the virus diffuses posteriorly to hit all PBN subnuclei; this injection site improves the accuracy of injecting into the lateral PBN between the superior cerebellar peduncle (scp) and lateral wall of the pons. Also note that the presence of the scp fortuitously limits the spread of virus from the PBN region, thus preventing unintended transduction of other nearby *Calca*-expressing brain regions.

After viral injection, mice used for optogenetic experiments also received unilateral surgical implantation of a Mono Fibreoptic Cannula (Doric Lenses), either above the PBN (AP, −5.2 mm; ML, 1.6 mm; DV, 3.0 mm), CeAlc (AP, −1.2 mm; ML, 2.6 mm; DV, 5.4 mm) or BNST (AP, +0.14 mm; ML, 1.0 mm; DV, 4.0 mm). Cannulae were affixed to the skull with C&B Metabond (Parkell) and dental acrylic.

Slice electrophysiology. Coronal brain slices (250 μm) were prepared in an ice slush solution containing (in mM) 250 sucrose, 3 KCl, 2 $MgSO_4$, 1.2 NaH_2PO_4, 10 D-glucose, 25 $NaHCO_3$ and 0.1 $CaCl_2$. Slices recovered for 1 h at 34 °C in artificial cerebral spinal fluid (ACSF) continually bubbled with O_2/CO_2 and containing (in mM) 126 NaCl, 2.5 KCl, 1.2 NaH_2PO_4, 1.2 $MgCl_2$ 11 D-glucose, 18 $NaHCO_3$ and 2 $CaCl_2$. Whole-cell patch-clamp recordings were made using an Axopatch 700B amplifier (Molecular Devices) with filtering at 1 kHz using 4–6 MΩ electrodes filled with an internal solution containing (in mM) 120 $CsMeSO_3$, 20 HEPES, 0.4 EGTA, 2.8 NaCl, 5 Mg-ATP, 0.5 Na-GTP, pH 7.2–7.4, 280 mOsm (for CeAlc single EPSC recordings) or 135 $KMeSO_3$, 10 KCl, 10 HEPES, 0.1 EGTA, 2.8 NaCl, 5 Mg-ATP, 0.5 Na-GTP, pH 7.2–7.4, 280 mOsm (for PBN recordings and CeAlc high-frequency stimulus recordings). ACSF at 32 °C was continually perfused over slices at a rate of approximately 2 ml min^{-1} during recording.

For photostimulation experiments in the CeAlc, neurons surrounded by mCherry-positive fibres were selected for recording. For light-evoked EPSCs, neurons were held in voltage clamp at −70 mV, and EPSCs were stimulated by 10-ms pulses of blue laser light (single pulse or 300 pulses at 30 Hz) using the same fibre optic as for the *in vivo* experiments, placed in the bath above the slice. Traces are averages of 15–20 sweeps for single EPSCs or averages of three sweeps for 30 Hz trains, collected before and 5 min after bath application of CNQX (10 μM) and AP5 (50 μM). For CeAlc current clamp recordings, most CeAlc neurons had resting membrane potentials between −65 and −80 mV and did not fire action potentials spontaneously unless constant current was injected through the patch pipette to bring the cell closer to threshold. Trains of stimuli at 30 Hz were delivered as above.

For PBN ChR2 recordings, neurons identified by fluorescence were recorded in current-clamp mode and trains of light pulses (1 ms) were delivered at the indicated frequencies for durations of 2 s. For pharmacogenetic experiments, neurons expressing hM_4Di were identified by fluorescence. Cells that did not show spontaneous firing were excluded. Neurons were recorded in current clamp mode in ACSF for a 5-min baseline period, followed by bath application of 3 μM CNO for 3 min, then washout with ACSF. Baseline firing rate was calculated from a 2-min window immediately before CNO application. CNO and washout firing rates were calculated from 2-min windows surrounding the maximum CNO effect and the maximum recovery period, respectively.

Food intake monitoring. For feeding assays, mice were individually housed in lickometer cages (Columbus Instruments) supplied with water and liquid diet (Vanilla Ensure, Abbot Laboratories) available *ad libitum*. Food and water ports were changed daily at the start of the dark cycle. The mice were allowed to acclimate to lickometer cages for 5 days and then baseline food intake was measured for an extra 5 days before experimental procedures. Acute food intake measurements (Figs 2b, c, e, f, 3b and 4d, f) occurred at the onset of the active period (lights off). Long-term measurements (Fig. 2g, h and 3c, d) occurred over a 24-h period with total food-intake and body weight measured approximately 6 h before the onset of the active period. Measurements were performed by an investigator (M.E.C.) with knowledge of the identity of the experimental versus control groups (that is, without blinding).

Photostimulation. After a 14-day recovery period following surgery, mice were individually housed in lickometer cages with open cage tops. Fibre optic cables (1.5 m long, 200 μm diameter; Doric Lenses) coated with opaque heat-shrink tubing were firmly attached to the implanted fibre optic cannulae with zirconia sleeves (Doric Lenses). Mice were allowed at least 5 days to acclimate before experimental sessions. During photostimulation experiments, light pulse trains (10-ms pulses of various frequency; see text) were programmed using a waveform generator (Agilent Technologies, number 33220A) that provided input to a blue light laser (473 nm; LaserGlow). We adjusted the light power of the laser such that the light power exiting the fibre optic cable was 20 mW (160 mW mm^{-2}); using an online light transmission calculator for brain tissue[33] (http://www.stanford.edu/group/dlab/cgi-bin/graph/chart.php) we estimated the light power at the PBelo to be 36.2 mW mm^{-2}. Note that this is probably a high estimation because some light was probably lost at the interface between the fibre optic cable and the implanted fibre optic cannula. After the completion of photostimulation experiments, mice were perfused and the approximate locations of fibre tips were identified based on the coordinates of Paxinos and Franklin[32].

Pharmacological injections. Pharmacological compounds were prepared in sterile 0.9% saline and stored at −20 °C before use. Diphtheria toxin was injected intramuscularly and all other compounds were administered intraperitoneally as described in Supplementary Fig. 6. Compounds included amylin (10 μg kg^{-1}; Bachem, number H-9475), CCK-8 (10 μg kg^{-1}; Bachem, number H-2080), CNO (1 mg kg^{-1}; Sigma, number C0832), diphtheria toxin (50 μg kg^{-1}; List Biologicals, number 150), LiCl (84 mg kg^{-1}; 0.20 M at 10 ml kg^{-1}; Fisher, number L121) and LPS, *S. typhimurium* (50 μg kg^{-1}; Calbiochem, number 437650).

Histology. Mice were anaesthetized with buprenorphine and perfused transcardially with 1× PBS, pH 7.4, followed by 4% paraformaldehyde in PBS. The brains were extracted, allowed to postfix overnight in the same fixative at 4 °C and cryoprotected in 30% sucrose dissolved in 1× PBS for an extra 24 h at 4 °C. Each brain was sectioned at 30 μm on a cryostat (Leica Microsystems) and collected in cold 1× PBS.

For immunohistochemistry experiments, sections were washed three times in PBS with 0.2% Triton X-100 (PBST) for 10 min at room temperature. Sections

were then incubated in a blocking solution composed of PBST with 3% normal donkey serum (Jackson ImmunoResearch, number 017-000-121) for 1 h. For primary antibody exposure, sections were incubated in rabbit anti-c-Fos (1:2000, Calbiochem, number PC38), rabbit anti-GFP (1:1000, Invitrogen, number A11122) and/or goat anti-CGRP (1:500, Abcam, number ab36001) in blocking solution at 4 °C for approximately 20 h. After three 10-min washes in PBST, sections were incubated in Alexa Fluor 594 donkey anti-goat IgG (1:200, Jackson Immunoresearch, number 705-858-147), Alexa Fluor 488 donkey anti-goat IgG (1:200, Jackson Immunoresearch, number 705-485-147), DyLight 405 donkey anti-goat (1:200, Jackson Immunoresearch, number 705-475-147) and/or Alexa Fluor 488 donkey anti-rabbit IgG (1:200 Jackson Immunoresearch, number 711-545-152) in block solution for 1 h at room temperature. Finally, sections were washed three times in 1× PBS.

Sections were mounted in PBS onto SuperFrost Plus glass slides (VWR, number 48311-703) and coverslipped with Dapi Fluoromount-G (Southern Biotech, number 0100-20). Slides were stored in the dark at 4 °C before microscopy and image acquisition.

Quantification of co-localization of Fos and mCherry in the PBN (Fig. 1c–j and Supplementary Fig. 7) was performed on adjacent sections from approximately Bregma −4.90 to −5.50 (exactly 21 sections per mouse). Quantification of Fos in the CeAlc (Supplementary Fig. 14a–f) was performed on adjacent sections from approximately Bregma −1.14 to −1.26 (exactly five sections per mouse). A Fos-positive cell was considered located in the CeAlc if it was in the field of mCherry fluorescence in that particular section. An investigator (M.E.C.) blinded to the identity of the conditions used to induce Fos performed all quantification.

Microscopy. Fluorescent and brightfield images were collected on either a Nikon upright epifluorescent microscope with a QImaging Camera (Figs 1b and 4a and Supplementary Figs 1 and 4) or a Zeiss LSM 510 Meta confocal microscope. Images were minimally processed using Photoshop CS5 (Adobe Systems) to enhance brightness and contrast for optimal representation of the data. Low-magnification brightfield images (Figs 1b and 4a and Supplementary Fig. 4) were montaged together to produce a single coronal section. All digital images were processed in the same way between experimental conditions to avoid artificial manipulation between different data sets.

Statistics. We used an online power and sample size calculator to determine an effective sample size for statistical comparisons[34] (http://homepage.cs.uiowa.edu/~rlenth/Power/). Assuming a standard deviation of 1.0 and a significance level of 0.05, this calculator shows that with eight mice per group we had an 80% confidence level of achieving statistical significance between means of 1.5-fold with a two-tailed Student's *t*-test. We excluded an animal from data analysis if flagged by a University of Washington veterinarian for health reasons during the experimental period or if *post hoc* histological analysis showed no viral transduction as indicated by an absence of mCherry fluorescence.

All data were analysed using Prism 6.0 (GraphPad Software) as described in the text and Supplementary Statistical Analysis. Data were exported into Illustrator CS5 (Adobe Systems) for preparation of figures.

31. Kremer, E. J., Boutin, S., Chillon, M. & Danos, O. Canine adenovirus vectors: an alternative for adenovirus-mediated gene transfer. *J. Virol.* **74,** 505–512 (2000).
32. Paxinos, G. & Franklin, K. B. J. *The Mouse Brain in Stereotaxic Coordinates* 4th edn (Elsevier, 2013).
33. Aravanis, A. *et al.* An optical neural interface: *in vivo* control of rodent motor cortex with integrated fiberoptic and optogenetic technology. *J. Neural Eng.* **4,** S143–S156 (2007).
34. Lenth, R. V. Some practical guidelines for effective sample size determination. *Am. Stat.* **55,** 187–193 (2001).

doi:10.1038/nature12596

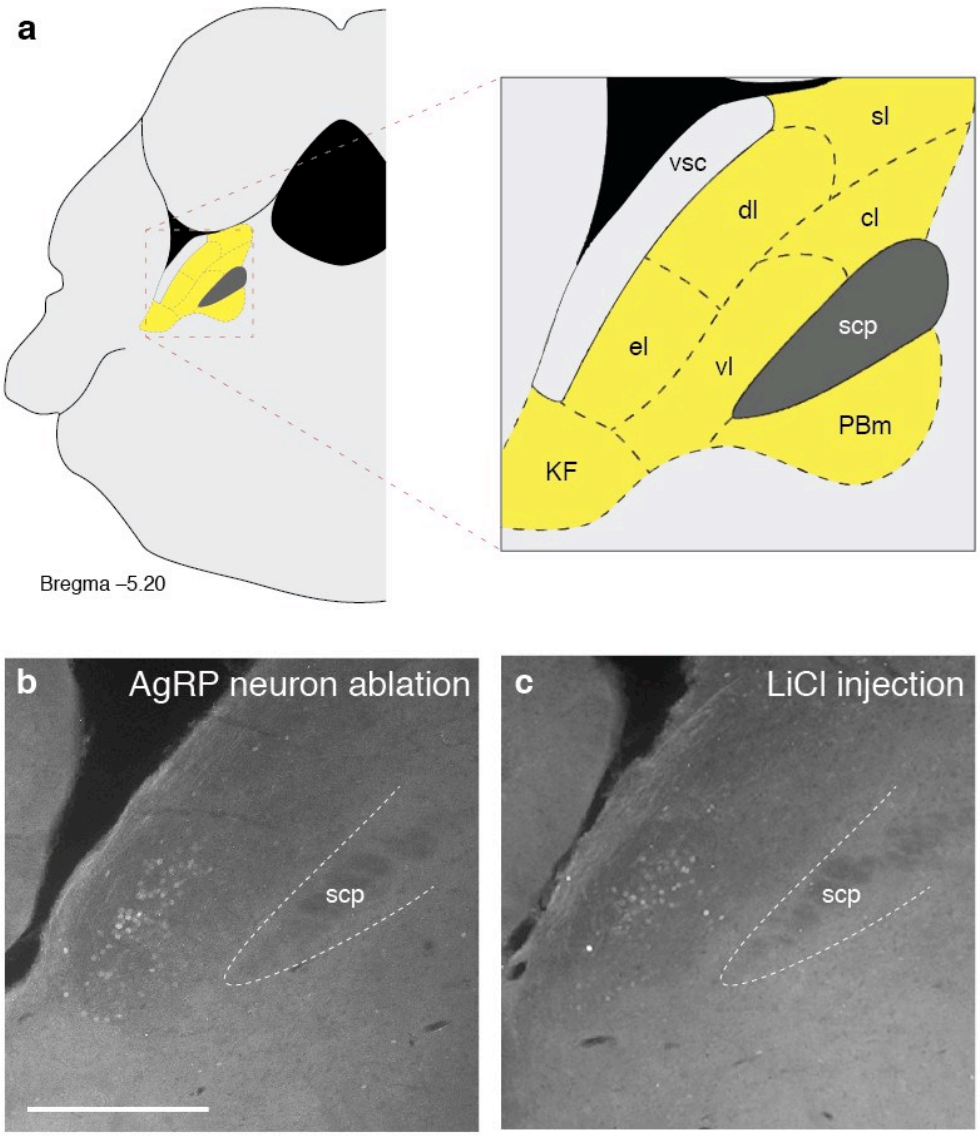

Supplementary Figure 1. Expression of Fos in the PBN following ablation of AgRP neurons or injection of LiCl. a, Diagram of a coronal section of the mouse brainstem based on structures delineated by the Allen Brain Atlas. **b, c,** Expression of Fos following genetic ablation of AgRP neurons (b) or injection of LiCl (c). cl, central lateral PBN, dl, dorsal lateral PBN; el, external lateral PBN; KF, Kolliker-Fuse nucleus; PBm, medial division of the PBN; scp, superior cerebellar peduncle; sl, superior lateral PBN; vl, ventral lateral PBN; vsc, ventral spinocereberllar tract. Scale bar, 500 μm.

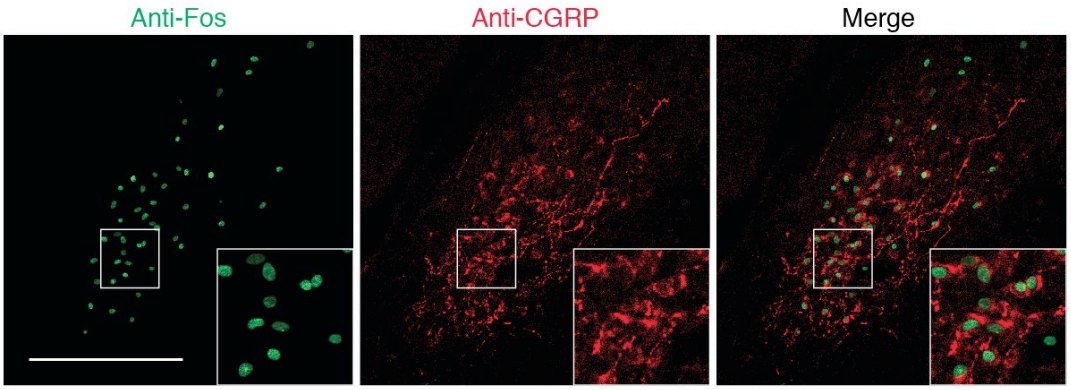

Supplementary Figure 2. Co-expression of Fos and CGRP immunofluorescence in the PBN following genetic ablation of AgRP neurons. Scale bar, 200 μm.

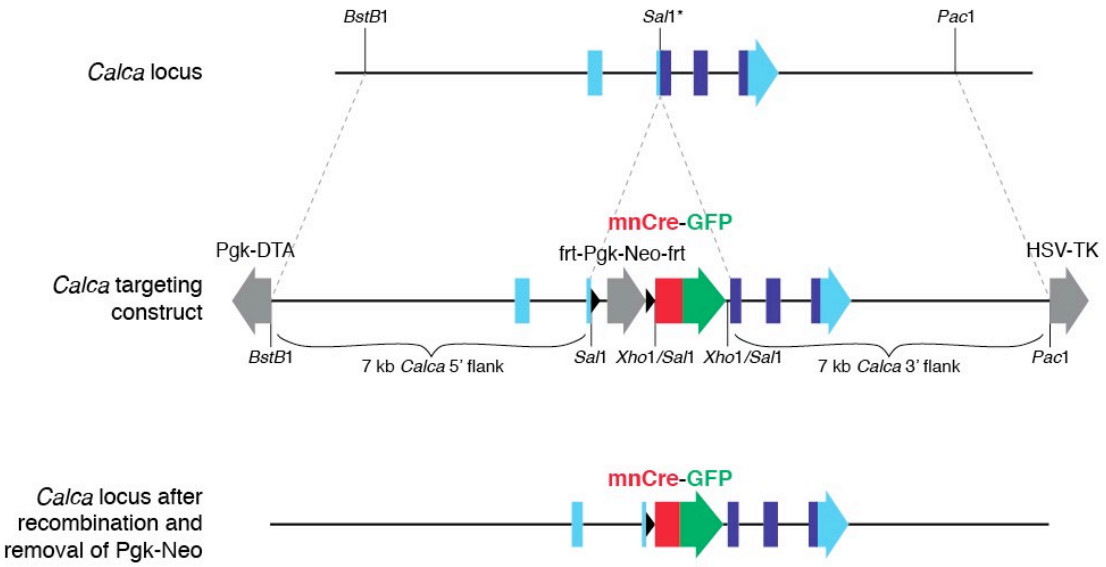

Supplementary Figure 3. Generation of *Calca*^{Cre} mice. Diagram showing: top, the *Calca* gene (4 exons with coding region in dark blue); middle, the targeting vector; and bottom, the *Calca* locus after recombination and removal of the *frt-Pgk-Neo* gene. The mnCre-GFP has a myc-tag and nuclear localization signal at the N-terminus of Cre and is fused in frame to EGFP at the C-terminus. Some key restriction enzyme sites used for cloning are shown. The *Sal*1* site at the initiation codon was introduced by PCR. Diagram is not to scale. See Supplementary Methods for details.

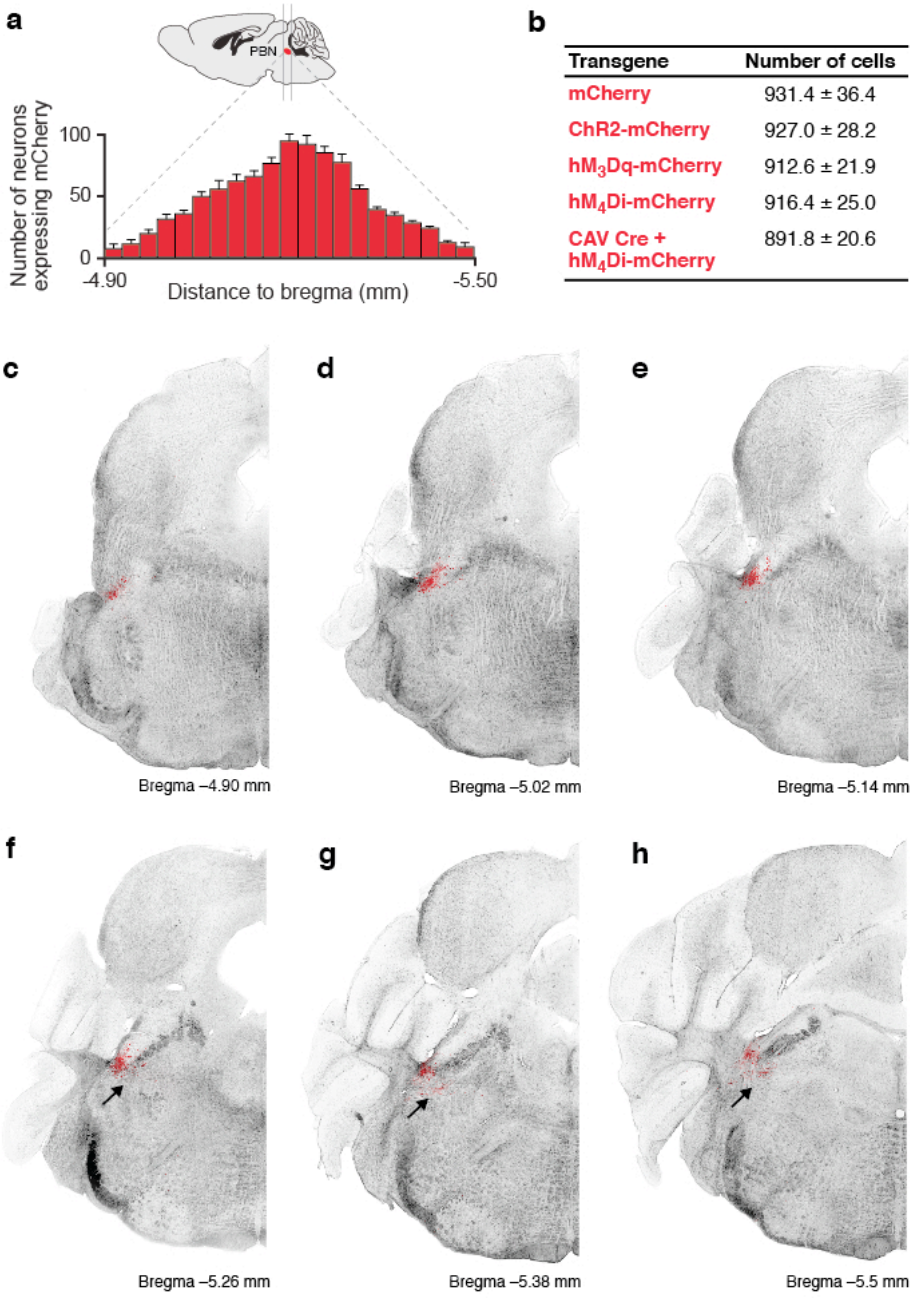

Supplementary Figure 4. Global analysis of virally-targeted PBN neurons. a, Number of neurons expressing mCherry in 21 coronal sections throughout the anteroposterior axis following injection of AAV1 DIO mCherry into *Calca*$^{Cre/+}$ mice. **b,** Mean number of mCherry-expressing neurons ± s.d. in animals injected with viral vectors used throughout this study. **c-h,** Representative coronal sections throughout the anteroposterior axis in a single *Calca*$^{Cre/+}$animal injected with AAV1 DIO mCherry. Arrows show mCherry-positive fibers emanating from the PBN.

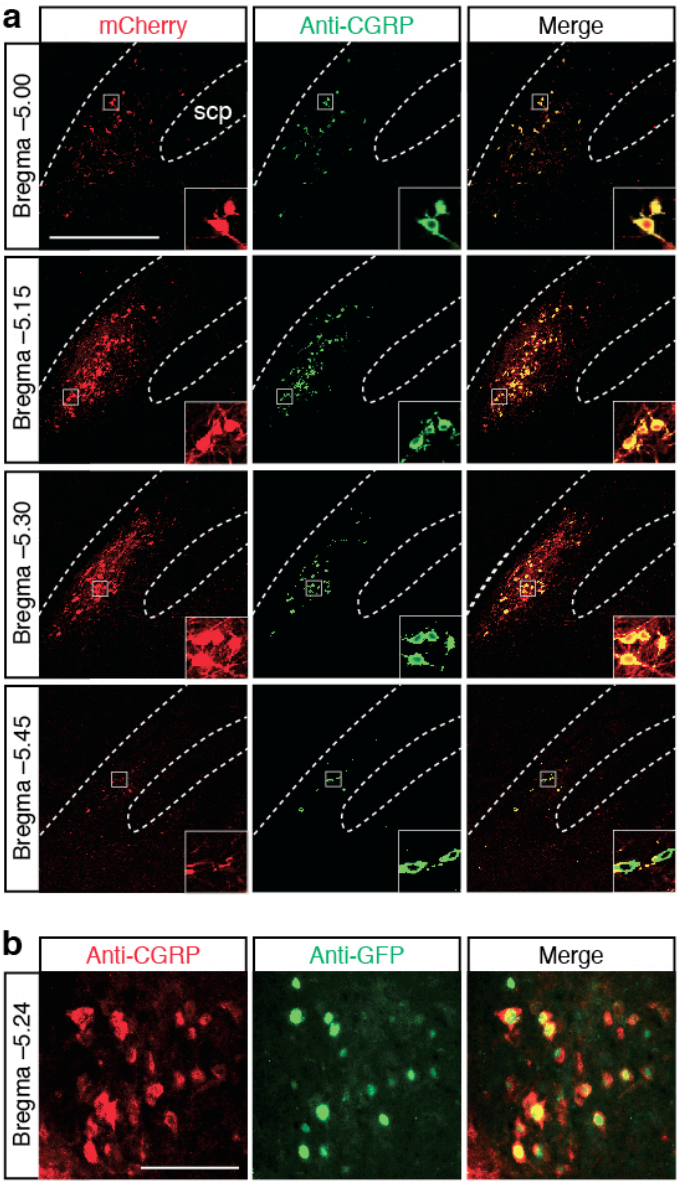

Supplementary Figure 5. Specificity of Cre expression and viral transduction in *Calca*^{Cre} mice. a, Representative sections through the anteroposterior axis of the PBN from a *Calca*$^{Cre/+}$ mouse injected with AAV1 DIO mCherry into the PBN and stained for CGRP. scp, superior cerebellar peduncle; scale bar, 500 µm. **b,** Representative section of the PBN from a *Calca*$^{Cre/+}$ mouse stained for CGRP and GFP; scale bar, 200 µm. Note that GFP fluorescence was not detectable without immunohistochemical amplification.

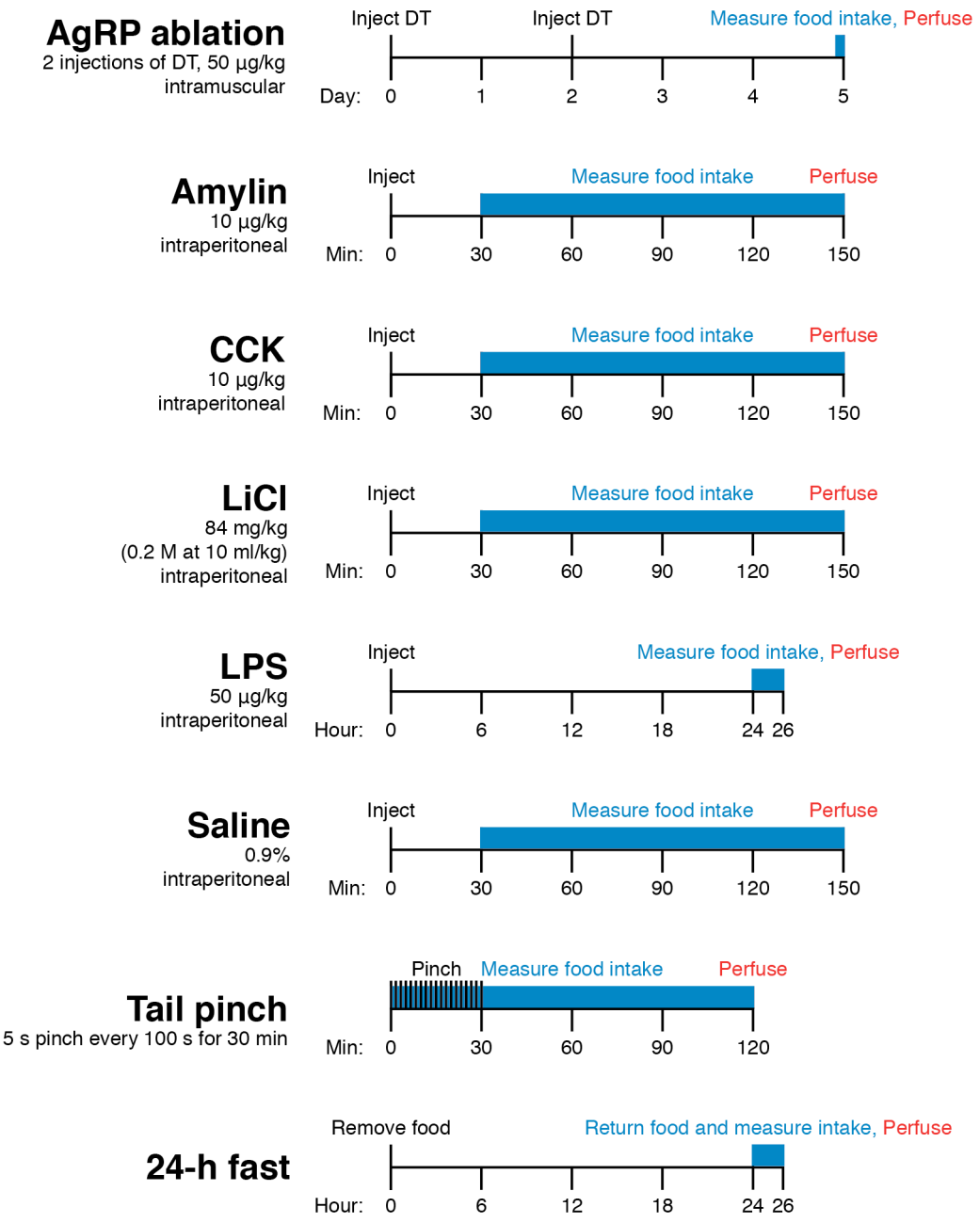

Supplementary Figure 6. Summary of procedures used to reduce food intake. See Supplementary Methods for further details.

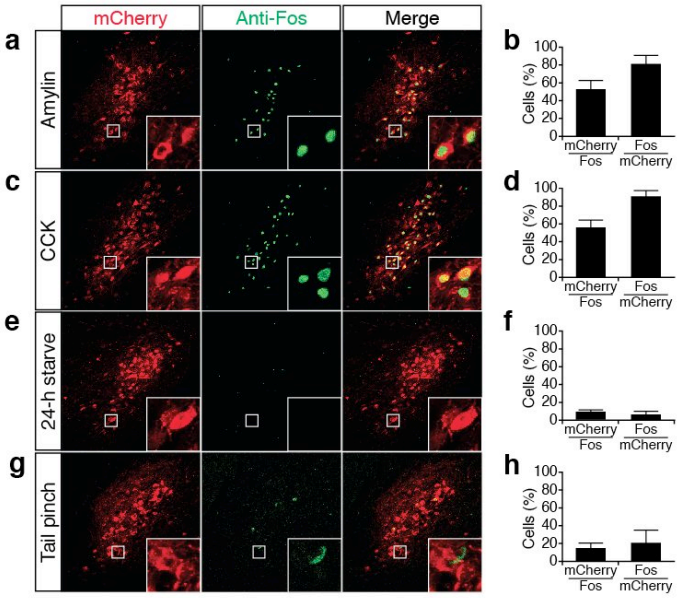

Supplementary Figure 7. Co-localization of PBelo CGRP neurons with Fos following conditions that reduce food intake. Representative histological examples and quantification of coincidence of mCherry and Fos expression in the PBN following amylin injection, CCK injection, 24-h fast, and tail pinch (see Supplementary Fig. 6 for summary of conditions to induce Fos; See Fig. 1 for additional conditions). Quantitative data represent mean ± standard error of the mean (s.e.m.).

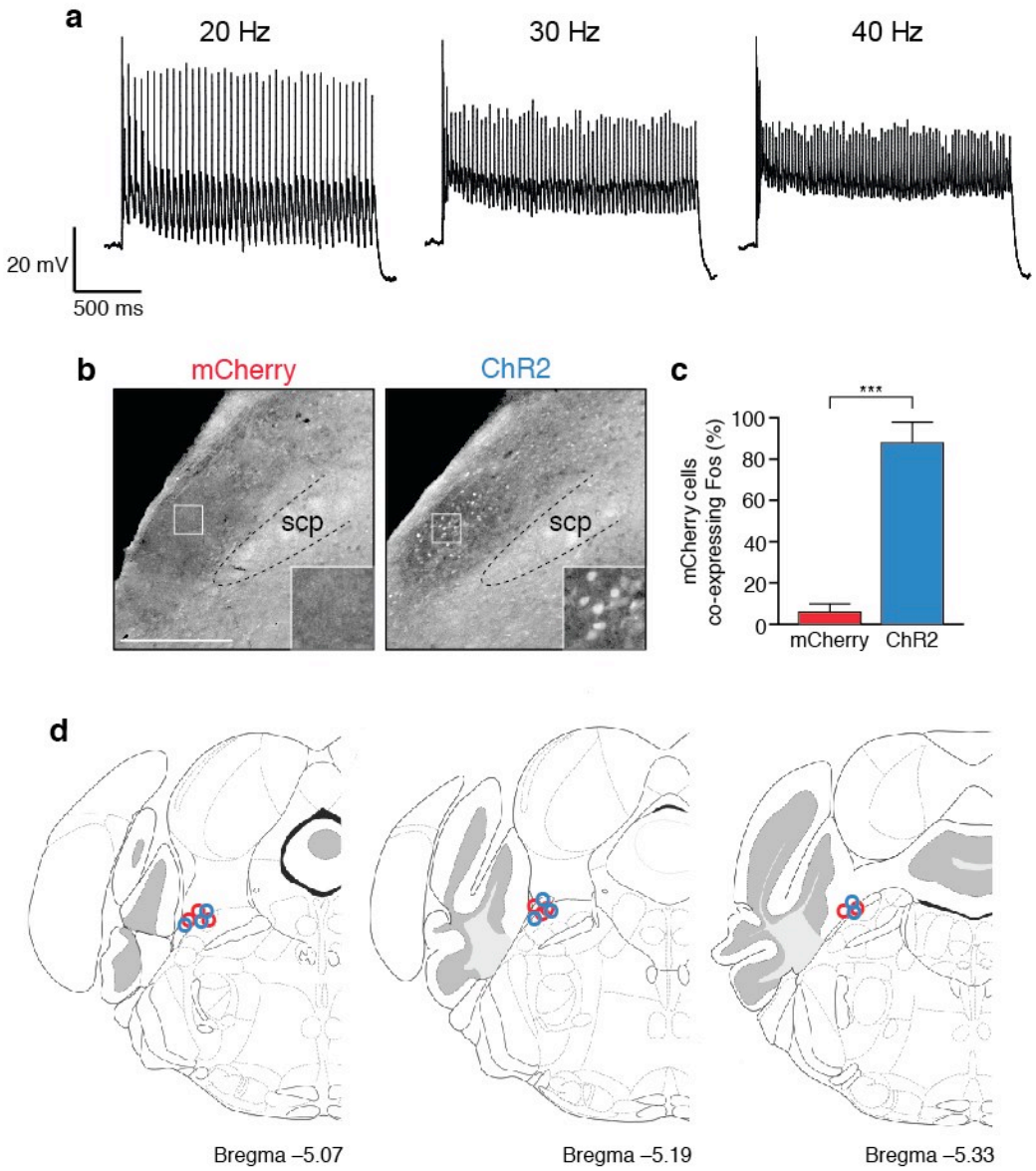

Supplementary Figure 8. Efficient functional expression of ChR2 in PBelo CGRP neurons. **a,** Example action potential trains evoked in acute brainstem slices by photostimulation of ChR2-positive PBelo neurons at the indicated frequencies. **b,** Representative sections from mCherry- or ChR2-mCherry-transduced animals following 5-min blue light stimulation (5 min at 30 Hz, 10-ms pulses) and subsequent immunohistochemical staining for Fos. Scale bar, 500 μm**. c,** Quantification of the percentage of mCherry-expressing neurons in the PBN co-expressing Fos. Data represent mean ± s.d.; ***P < 0.001; See Supplementary Information for statistical analyses. **d,** Approximate locations of fiber optic implants for photostimulation experiments (Fig. 2b,c) among animals transduced with mCherry (red circles) or ChR2-mCherry (blue circles).

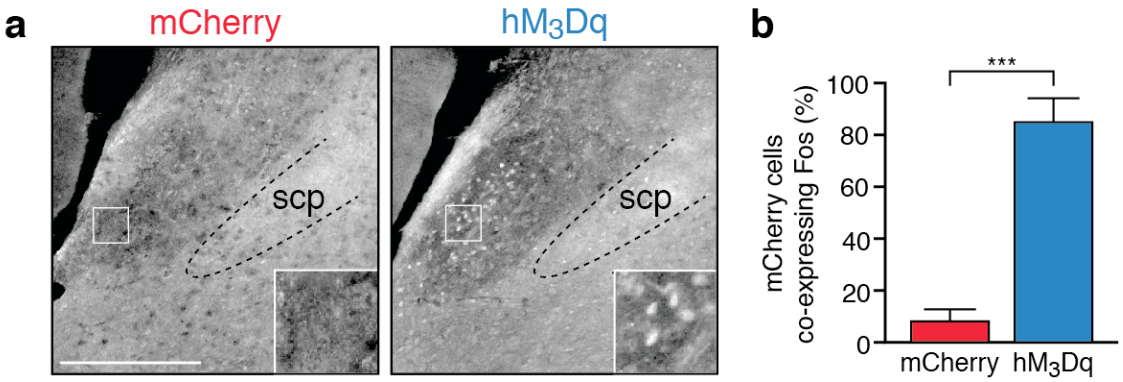

Supplementary Figure 9. Efficient functional expression of hM_3Dq in PBelo CGRP neurons. **a,** Representative sections from mCherry- or hM_3Dq-mCherry-transduced animals following i.p. injection of CNO (1.0 mg/kg) and subsequent immunohistochemical staining for Fos. Scale bar, 500 µm**.** **b,** Quantification of the percentage of mCherry-expressing neurons in the PBN co-expressing Fos. Data represent mean ± s.d.; ***P < 0.001; See Supplementary Information for statistical analyses.

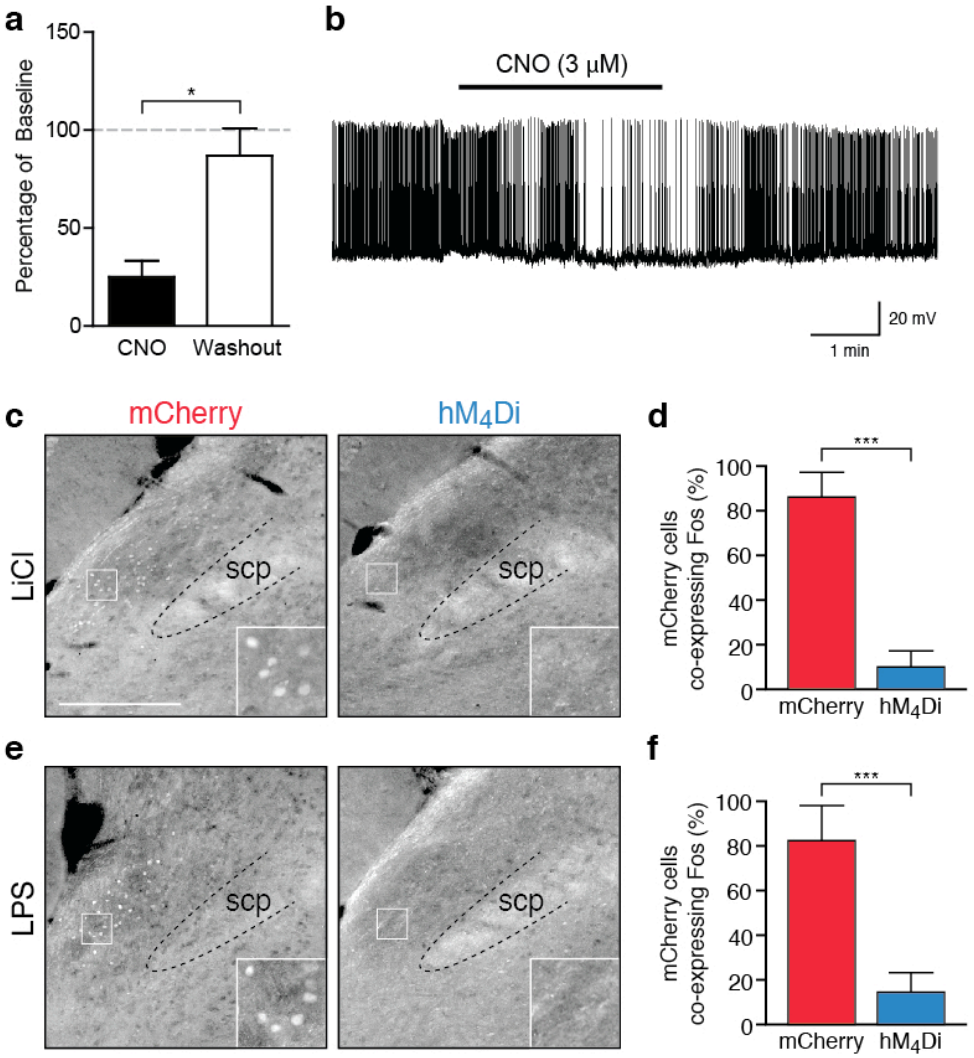

Supplementary Figure 10. Efficient functional expression of hM$_4$Di in PBelo CGRP neurons. **a,** Firing rate (relative to baseline) of hM$_4$Di-transfected PBelo neurons following bath application of 3 μM CNO and washout of CNO. Data represent mean ± s.e.m.; *P < 0.05. **b,** Representative trace showing action potential firing before, during, and after washout of CNO application in an acute brain slice. **c, e,** Representative sections from mCherry- or hM$_4$Di-mCherry-transduced animals following i.p injection of either LiCl (c) or LPS (e) with concurrent i.p. injection of CNO (1.0 mg/kg) and subsequent immunohistochemical staining for Fos. Scale bar 500 μm. **d, f,** Quantification of the percentage of mCherry-expressing neurons in the PBN co-expressing Fos following injection of LiCl (d) or LPS (f). Data represent mean ± s.d.; ***P < 0.001; See Supplementary Information for statistical analyses.

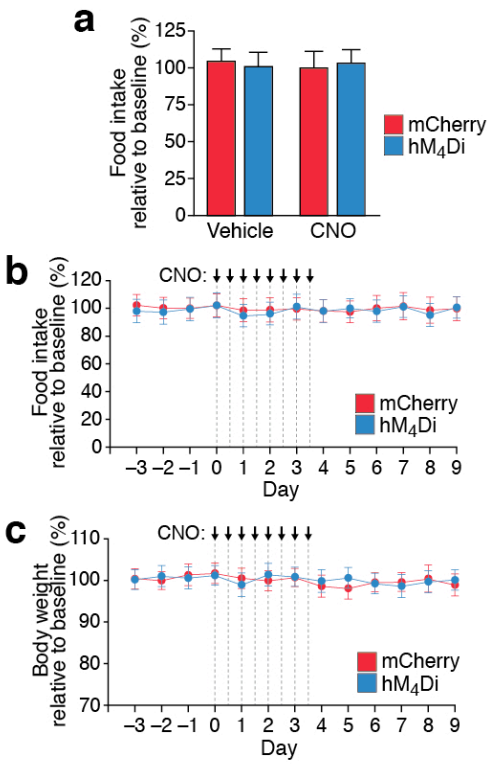

Supplementary Figure 11. Inhibition of PBelo CGRP neurons with hM$_4$Di does not affect baseline food intake. **a,** Acute pharmacogenetic inhibition of CGRP neurons with CNO does not affect food intake. **b, c,** Chronic administration of CNO (every 12 h for 4 d) does not affect food intake (b) or body weight (c) in baseline conditions. Data represent mean ± s.e.m.; See Supplementary Information for statistical analyses.

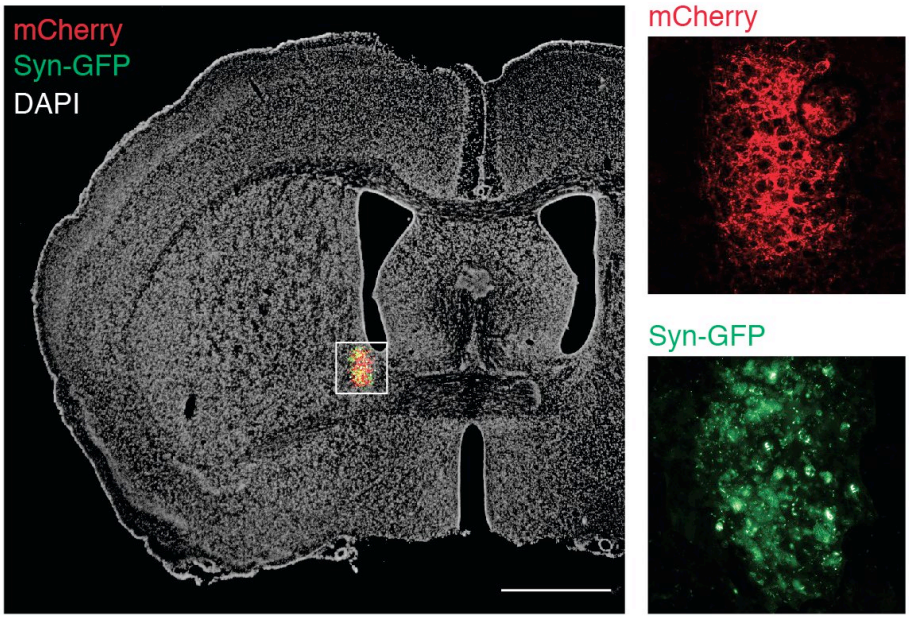

Supplementary Figure 12. Efferent projections of PBelo CGRP neurons to the bed nucleus of the stria terminalis (BNST). Representative section from a *Calca*$^{Cre/+}$ mouse injected with AAV DIO mCherry and AAV DIO Synaptophysin-GFP into the PBN. Bregma = +0.01 mm; Scale bar, 1 mm.

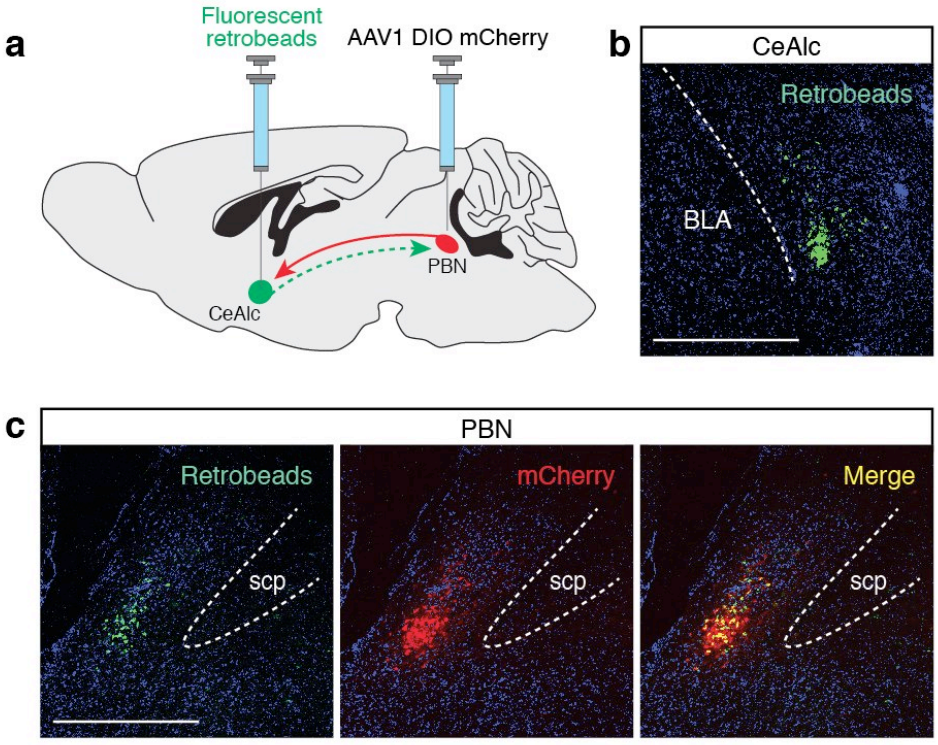

Supplementary Figure 13. Efferent projections from the PBN to the CeAlc originate from CGRP-expressing neurons in the PBelo. **a,** Diagram showing injection of green fluorescent retrobeads in the CeAlc and AAV DIO mCherry into the PBN of *Calca*$^{Cre/+}$ mice. **b,** Green retrobead injection in the CeAlc. BLA, basolateral amygdala. **c,** Overlap of green retrobeads with viral mCherry in the PBN. scp, superior cerebellar peduncle. Scale bars, 500 μm.

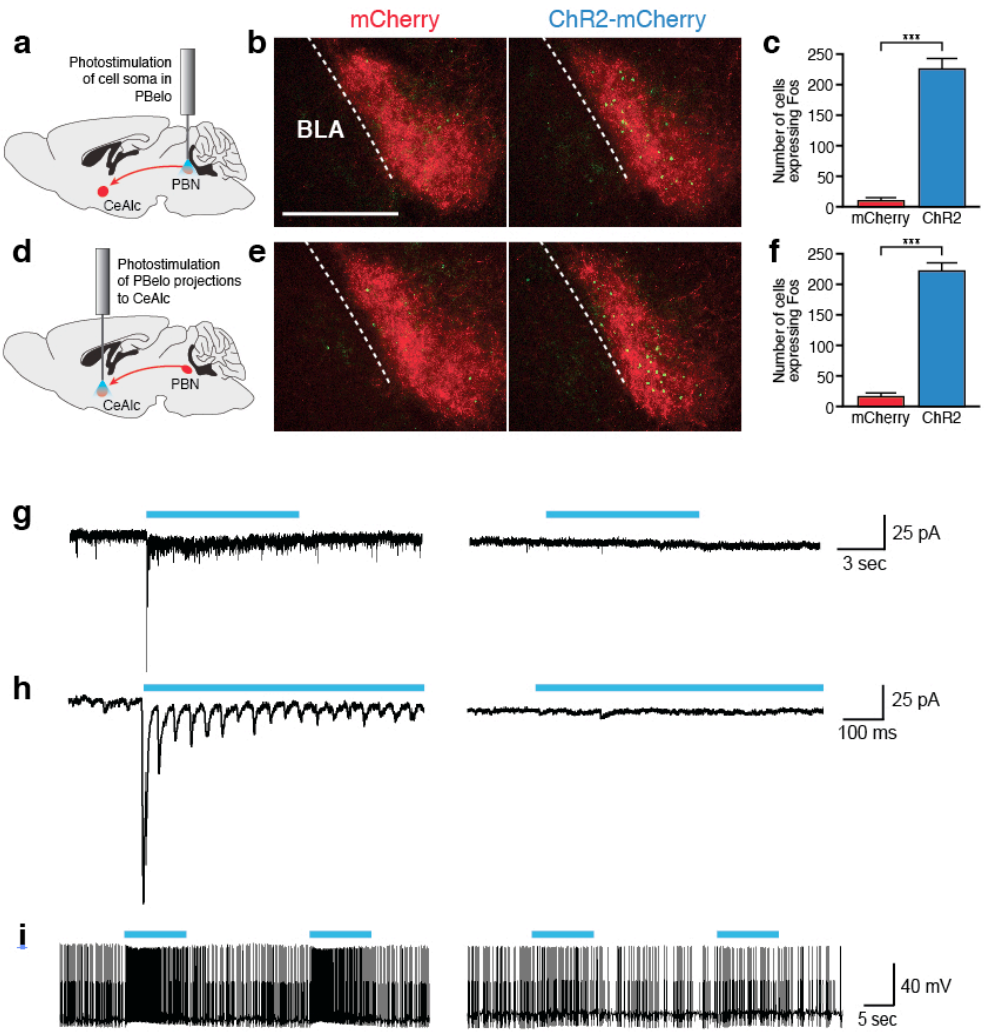

Supplementary Figure 14. Functional connectivity from PBelo CGRP neurons to the CeAlc. **a, d,** Diagrams depicting experimental conditions in b-c and e-f, respectively. **b, e,** Representative coronal sections through the CeAlc showing mCherry-expressing fibers (red) and Fos immunoreactivity (green) following photostimulation (5 min at 30 Hz, 10-ms pulses) in the PBelo (b) or CeAlc (e) from animals transduced with either mCherry or ChR2-mCherry in PBelo CGRP neurons. **c, f,** Quantification of the number of cells expressing Fos in (b) or (e), respectively. Data represent mean ± s.d.; ***P < 0.001; See Supplementary Information for statistical analyses. **g,** Representative current trace from a CeAlc neuron in slice upon photostimulation of PBelo-to-CeAlc fibers at 30 Hz (blue line) before (left) or after (right) bath application of CNQX and APV. **h,** Expanded view of current traces in (g) showing individual responses to light pulses. **i,** Representative current clamp traces showing action potentials in response to 30 Hz photostimulation (blue line) before (left) or after (right) bath application of CNQX and APV. Five out of seven cells showed an increase in firing rate greater than two-fold during 30 Hz photostimulation.

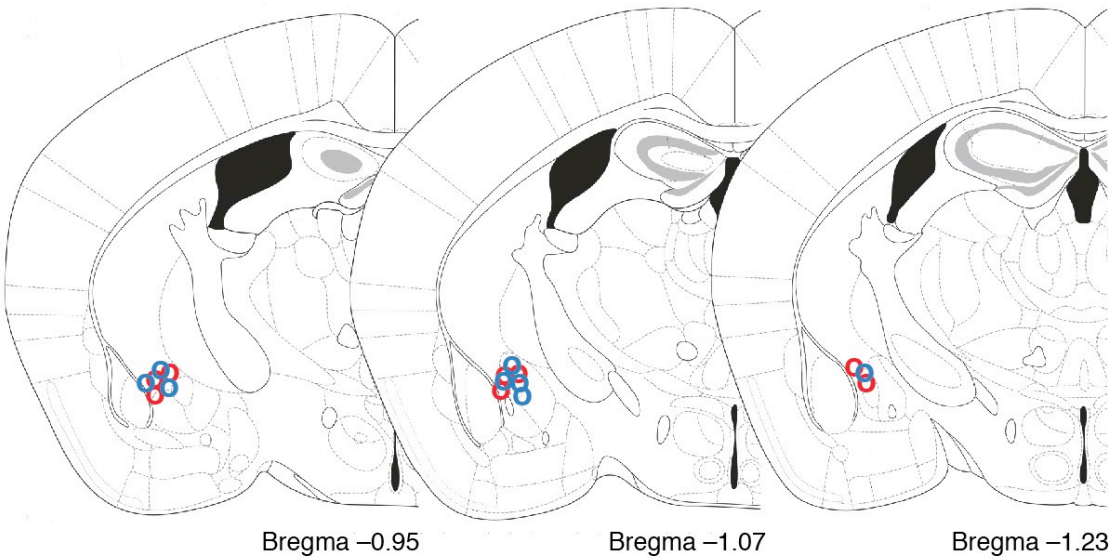

Supplementary Figure 15. Placement of fiber optic cannulae in the CeAlc.
Approximate locations of fiber optic implants for photostimulation experiments (Fig. 4d) among animals transduced with mCherry (red circles) or ChR2-mCherry (blue circles).

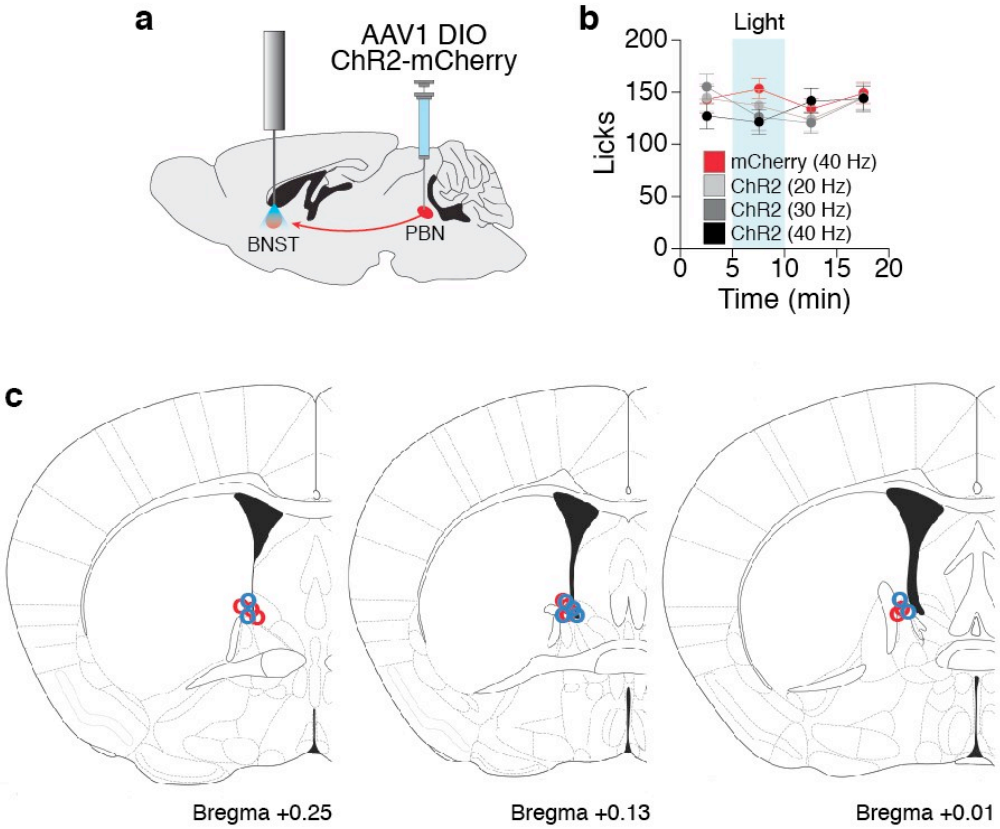

Supplementary Figure 16. Photostimulation of PBelo efferent projections to the BNST. **a,** Diagram showing transduction of PBelo CGRP neurons with ChR2-mCherry and placement of a fiber-optic cannula above the BNST. **b,** Photostimulation of PBelo CGRP fibers in the BNST has no significant effect on food intake. Data represent mean ± s.e.m.; See Supplementary Information for statistical analyses. **c,** Approximate locations of fiber optic implants for photostimulation experiments among animals transduced with mCherry (red circles) or ChR2-mCherry (blue circles).

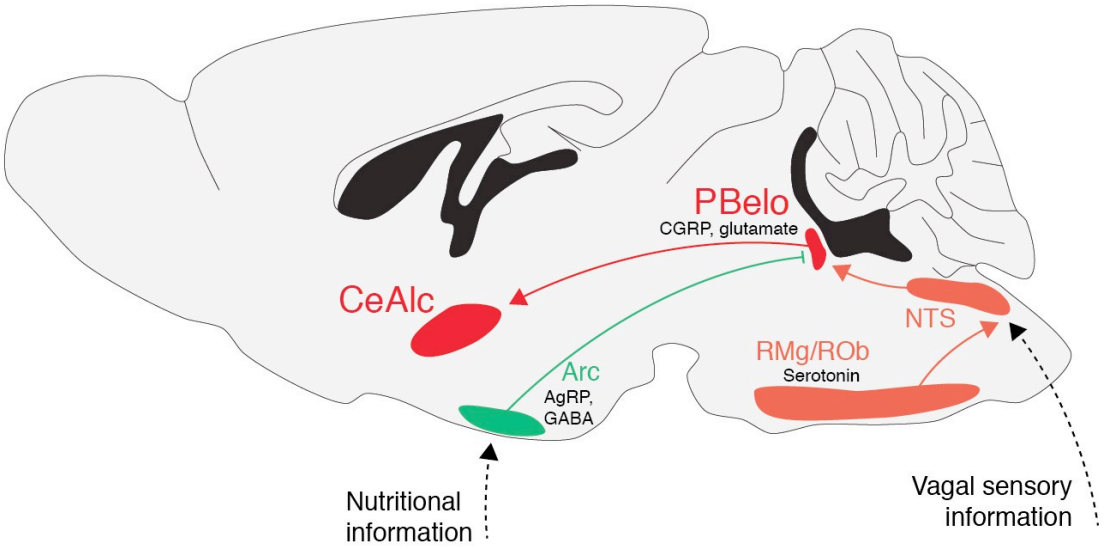

Supplementary Figure 17. Model of neural circuits that suppress appetite. The vagus nerve relays gustatory and enteric information from the viscera to the nucleus of the solitary tract (NTS). Serotoninergic neurons in the raphe magnus (RMg) and raphe obscurus (ROb) send excitatory projections to the NTS and contribute to appetite suppression[1]. NTS neurons project to the parabrachial nucleus, which also receives inhibitory projections from GABAergic, AgRP-expressing neurons in the hypothalamic arcuate nucleus (ARC)[8]. This study demonstrates that the relevant neurons in the PBN that suppress appetite express CGRP and send excitatory projections to the laterocapsular division of the central nucleus of the amygdala (CeAlc).

Supplementary Statistical Analysis

Figure 1d,f,h,j. n = 4 per condition. Data represent mean ± s.e.m.

Figure 1k. n = 32. Data represent mean ± s.e.m.

Figure 1l. n = 32. Spearman's rho = –0.86, $P < 0.0001$.

Figure 2b. n = 8 for each group. Data represent mean ± s.e.m. Total numbers of licks are binned in 5-min epochs. Two-way repeated measures ANOVA detected significant interaction of stimulation condition x epoch: $F_{9,84} = 3.437$, $P = 0.00120$. Bonferroni post-hoc test shows significant difference between ChR2-transduced animals (various frequencies) with mCherry-transduced control animals at indicated epochs.

Figure 2c. n = 8 for each group. Data represent mean ± s.e.m. Total numbers of licks are binned in 5-min epochs. Two-way repeated measures ANOVA detected significant interaction of stimulation condition x epoch: $F_{9,84} = 4.234$, $P = 0.00015$. Bonferroni post-hoc test shows significant difference between ChR2-transduced animals (various frequencies) with mCherry-transduced control animals at indicated epochs.

Figure 2e. n = 6 for each group. Data represent mean ± s.e.m. Two-way repeated measures ANOVA detected significant interaction of viral genotype x pharmacological agent: $F_{1,10} = 14.72$, $P = 0.00328$. Bonferroni post-hoc test shows significant difference between hM_3Dq-transduced animals with mCherry-transduced control animals as indicated.

Figure 2f. n = 6 for each group. Data represent mean ± s.e.m. Two-way repeated measures ANOVA detected significant interaction of viral genotype x pharmacological agent: $F_{1,10} = 20.874$, $P = 0.00103$. Bonferroni post-hoc test shows significant difference between hM_3Dq-transduced animals with mCherry-transduced control animals as indicated.

Figure 2g. n = 6 for each group. Data represent mean ± s.e.m. Two-way repeated measures ANOVA detected significant interaction of viral genotype x day: $F_{12,120} = 4.426$, $P = 0.0000008$. Bonferroni post-hoc test shows significant difference between hM_3Dq-transduced animals with mCherry-transduced control animals on days 2-6 as indicated.

Figure 2h. n = 6 for each group. Data represent mean ± s.e.m. Two-way repeated measures ANOVA detected significant interaction of viral genotype x day: $F_{12,120} = 5.763$, $P = 0.00000009$. Bonferroni post-hoc test shows significant difference between hM_3Dq-transduced animals with mCherry-transduced control animals on days 1-4 as indicated.

Figure 3b. n = 6 for each group. Data represent mean ± s.e.m. Two-way repeated measures ANOVA detected significant interaction of group x condition: $F_{4,50} = 3.685$, $P = 0.01048$. Bonferroni post-hoc test shows significant difference between hM_4Di-transduced animals and mCherry-transduced control animals as indicated.

Figure 3c. n = 6 hM_4Di-transduced animals n=9 mCherry-transduced animals. Data represent mean ± s.e.m. Two-way repeated measures ANOVA detected significant interaction of viral genotype x day: $F_{11,143} = 4.885$, P = 0.000002. Bonferroni post-hoc test shows significant difference between hM_3Dq-transduced animals with mCherry-transduced control animals on days 5-8 as indicated.

Figure 3d. n = 6 hM_4Di-transduced animals n=9 mCherry-transduced animals. Data represent mean ± s.e.m. Two-way repeated measures ANOVA detected significant interaction of viral genotype x day: $F_{11,143} = 2.954$, P = 0.00148. Bonferroni post-hoc test shows significant difference between hM_3Dq-transduced animals with mCherry-transduced control animals on days 5-8 as indicated.

Figure 4d. n = 8 for each group. Data represent mean ± s.e.m. Total numbers of licks are binned in 5-min epochs. Two-way repeated measures ANOVA detected significant interaction of stimulation condition x epoch: $F_{9,84} = 3.061$, P = 0.00322. Bonferroni post-hoc test shows significant difference between ChR2-transduced animals (various frequencies) with mCherry-transduced control animals at indicated epochs.

Figure 4f. n = 6 for each group. Data represent mean ± s.e.m. Two-way repeated measures ANOVA detected significant interaction of group x condition: $F_{2,20} = 5.260$, P = 0.01460. Bonferroni post-hoc test shows significant difference between hM_4Di-transduced animals and mCherry-transduced control animals as indicated.

Supplementary 4a,b. n = 5 per condition. Cells were counted in exactly 21 sections per animal. Data represent mean ± s.d.

Supplementary Figure 7b,d,f,h. n = 4 per condition. Data represent mean ± s.e.m.

Supplementary Figure 8c. n = 4 per condition. Data represent mean ± s.d. P = 0.00053, Student's t-test between viral genotype.

Supplementary Figure 9b. n = 4 per condition. Data represent mean ± s.e.m. P = 0.00044, Student's t-test between viral genotype.

Supplementary Figure 10a. n = 5 cells (one cell was excluded from analysis because it did not show any recovery after CNO washout). Data represent mean ± s.e.m. P = 0.012, Paired t-test between CNO and washout conditions.

Supplementary Figure 10d. n = 4 per condition. Data represent mean ± s.d. P = 0.00029, Student's t-test between viral genotype.

Supplementary Figure 10f. n = 4 per condition. Data represent mean ± s.d. P = 0.00039, Student's t-test between viral genotype.

Supplementary Figure 11a. n=6 for each group. Data represent mean ± s.e.m. Two-way repeated measures ANOVA did not detect significant interaction of viral genotype x pharmacological agent: $F_{1,10} = 2.963$, P = 0.11592.

Supplementary Figure 11b. n=6 for each group. Data represent mean ± s.e.m. Two-way repeated measures ANOVA did not detect significant interaction of viral genotype x day: $F_{12,120} = 1.422$, $P = 0.1650$.

Supplementary Figure 11c. n=6 for each group. Data represent mean ± s.e.m. Two-way repeated measures ANOVA did not detect significant interaction of viral genotype x day: $F_{12,120} = 1.007$, $P = 0.4469$.

Supplementary Figure 14c. n = 4 per condition. Data represent mean ± s.d. P = 0.00064, Student's t-test between viral genotype.

Supplementary Figure 14f. n = 4 per condition. Data represent mean ± s.d. P = 0.00014, Student's t-test between viral genotype.

Supplementary Figure 16b. n=8 for each group. Data represent mean ± s.e.m. Total numbers of licks are binned in 5-min epochs. Two-way repeated measures ANOVA did not detect significant interaction of stimulation condition x epoch: $F_{9,84} = 1.372$, $P = 0.21387$.